The Astrophysical Journal, 618:237–246, 2005 January 1

MASSES OF STAR CLUSTERS IN THE NUCLEI OF BULGELESS SPIRAL GALAXIES

C. J. Walcher,[1] R. P. van der Marel,[2] D. McLaughlin,[2] H.-W. Rix,[1] T. Böker,[3] N. Häring,[1]
L. C. Ho,[4] M. Sarzi,[5] and J. C. Shields[6]
Received 2004 July 8; accepted 2004 September 9

ABSTRACT

In the last decade star clusters have been found in the centers of spiral galaxies across all Hubble types. We here present a spectroscopic study of the exceptionally bright (10^6–$10^8\ L_\odot$) but compact ($r_e \sim 5$ pc) nuclear star clusters in very late type spirals with the Ultraviolet and Visual Echelle Spectrograph at the VLT. We find that the velocity dispersions of the nine clusters in our sample range from 13 to 34 km s^{-1}. Using photometric data from the *Hubble Space Telescope* WFPC2 and spherically symmetric dynamical models, we determine masses between 8×10^5 and $6 \times 10^7\ M_\odot$. The mass-to-light ratios range from 0.2 to 1.5 in the *I* band. This indicates a young mean age for most clusters, in agreement with previous studies. Given their high masses and small sizes, we find that nuclear clusters are among the objects with the highest mean surface density known (up to $10^5\ M_\odot$ pc^{-2}). From their dynamical properties we infer that, rather than small bulges, the closest structural kin of nuclear clusters appear to be massive compact star clusters. This includes such different objects as globular clusters, "super star clusters," ultracompact dwarf galaxies (UCDs), and the nuclei of dwarf elliptical galaxies. It is a challenge to explain why, despite the widely different current environments, all different types of massive star clusters share very similar and structural properties. A possible explanation links UCDs and massive globular clusters to nuclear star clusters through stripping of nucleated dwarf galaxies in a merger event. The extreme properties of this type of cluster would then be a consequence of the clusters' location in the centers of their respective host galaxies.

Subject headings: galaxies: nuclei — galaxies: spiral — galaxies: star clusters — galaxies: structure

1. INTRODUCTION

In the last decade the image quality of the *Hubble Space Telescope* (*HST*) has boosted the study of the centers of spiral galaxies. These observations have shown that star clusters are a common feature in the nuclei of spiral galaxies of all Hubble types (Phillips et al. 1996; Matthews & Gallagher 1997; Carollo et al. 1997, 1998; Böker et al. 2002), from bulge-dominated galaxies to bulgeless galaxies. Nuclear star clusters are hard to observe in early-type spirals against the bright bulge. However, in late-type, bulgeless galaxies, they stand out well against the low surface brightness disk. The *HST* survey by Böker et al. (2002, hereafter B02) has shown that 75% of all late-type spirals host such a nuclear cluster in their photometric center. We use the term nuclear cluster (NC) for a luminous and compact star cluster near the overall photometric center of the galaxy. While the effective radii ($\sim$5 pc; Böker et al. 2004, hereafter B04) are comparable to globular clusters, the luminosities exceed those of the most luminous Milky Way globular clusters by up to 2 orders of magnitude.

In the absence of any obvious bulge (Böker et al. 2003), NCs represent the closest thing to a central "hot component." In most galaxy formation scenarios the bulge at the center is the "trashbin of violent relaxation," where a kinematically hot stellar component has formed either through external potential perturbations, such as early mergers of fragments, or perhaps through internal effects, such as violent bar instabilities. Bulgeless galaxies, in contrast, must have lived very sheltered lives, as their central "trashbin" is virtually empty. The discovery of almost ubiquitous NCs at the same physical location in their host galaxy as a bulge would have been, brings up the question of whether bulges and NCs are related. A thinkable scenario would be that NCs are protobulges that grow by repeated accretion of gas and subsequent star formation. The pace of that growth and the resulting size of the central component would then determine whether we call the central component an NC or a small bulge.

While the high spatial resolution of *HST* allows surface photometry of the clusters, other fundamental parameters such as age and mass remain largely unknown. Several case studies in the literature, however, have revealed massive, young objects. M33 is the nearest Sc galaxy hosting an NC, and its nucleus has been extensively studied in the past decade (e.g., Davidge 2000; Long et al. 2002; Stephens & Frogel 2002). Despite some differences in the details, all studies on M33 agree that there is some population younger than 0.5 Gyr in the central parsec and that star formation has varied significantly over the past several Gyr. The mass of the central cluster in M33 was estimated from a detailed population analysis in Gordon et al. (1999) to be $5 \times 10^5\ M_\odot$, consistent with the upper limit derived from the velocity dispersion by Kormendy & McClure (1993) of $2 \times 10^6\ M_\odot$. From Hα rotation curves of late-type spirals, Matthews & Gallagher (2002) find that the velocity offsets at the position of five semistellar nuclei—certainly to be identified with NCs—are consistent with masses of $\approx 10^6$–$10^7\ M_\odot$. They also point out that the location of the cluster and the dynamical center of the galaxy do not always coincide. The only direct mass determination for an NC from a measurement of the stellar velocity dispersion and detailed dynamical modeling was done for the NC in IC 342 by Böker et al. (1999); they find $6 \times 10^6\ M_\odot$, with a *K*-band mass-to-light ratio of 0.05 in solar units. The derived

[1] Max Planck Institut für Astronomie, Königstuhl 17, D-69117 Heidelberg, Germany.
[2] Space Telescope Science Institute, 3700 San Martin Drive, Baltimore, MD 21218.
[3] ESA/ESTEC, Keplerlaan 1, 2200 AG Noordwijk, Netherlands.
[4] The Observatories of the Carnegie Institution of Washington, 813 Santa Barbara Street, Pasadena, CA 91101-1292.
[5] Oxford Astrophysics, Keble Road, Oxford OX1 3RH, UK.
[6] Department of Physics and Astronomy, Clippinger Research Laboratories, Ohio University, 251B, Athens, OH 45701-2979.

TABLE 1
Sample and Observations

Galaxy (1)	Type (2)	Distance (Mpc) (3)	m_I (4)	M_I (5)	S/N (6)	Contamination (%) (7)
NGC 300	SAd	2.2	15.29	−11.43	37	0
NGC 428	SABm	16.1	17.95	−13.15	16	30
NGC 1042	SABcd	18.2	18.40	−12.95	24	81
NGC 1493	SBcd	11.4	17.17	−11.43	20	33
NGC 2139	SABcd	23.6	19.28	−12.65	19	89
NGC 3423	SAcd	14.6	19.04	−11.84	15	76
NGC 7418	SABcd	18.4	15.12	−16.23	41	18
NGC 7424	SABcd	10.9	18.80	−11.41	16	77
NGC 7793	SAd	3.3	14.00	−13.64	65	0

Notes.—Cols. (1) and (2): Galaxy name and type as taken from NED. Col. (3): Distances were taken from B02, where they were calculated from the recession velocity (from LEDA, corrected for Virgocentric infall) and assume $H_0 = 70$ km s^{-1}. Cols. (4) and (5): Apparent and absolute magnitude of the NC as taken from Böker et al. (2002). Col. (6): S/N per pixel (∼0.07 Å) in the region around the calcium triplet. Col. (7): Contamination from galaxy disk light, measured as described in § 2.3.

mean age is $\leq 10^8$ yr. Böker et al. (2001) also studied the NC in NGC 4449 using population synthesis models. They estimate an age of $\approx 10^7$ yr, in agreement with Gelatt et al. (2001). They infer a lower limit for the mass, which is $4 \times 10^5\ M_\odot$.

The available sizes, masses, and ages suggest kinship between NCs and either globular clusters (GCs), super star clusters (SSCs), or the nuclei of dwarf elliptical (dE) galaxies. Alternatively, NCs could be a new class of objects that would then be part of the wide range of special phenomena occurring in galaxy centers. To establish the relation between these objects, we clearly need reliable determinations of the velocity dispersion σ and therefore masses as well as ages for a statistically significant sample of objects. This is the first paper in a series of two describing the results of ground-based follow-up spectroscopy with the Ultraviolet and Visual Echelle Spectrograph (UVES) at the VLT to the *HST* survey by Böker et al. (2002). Here we focus on the masses and velocity dispersions of the NCs, while a second paper (C. J. Walcher et al. 2005, in preparation) will deal with ages and stellar populations.

2. SAMPLE SELECTION AND DATA

2.1. *Sample Selection*

All objects were drawn from the sample in B02. Galaxies in this survey were selected to have Hubble type between Scd and Sm, to have line-of-sight velocity $v_{\rm hel} < 2000$ km s^{-1}, and to be nearly face-on. A subset of nine objects (listed in Table 1) were observed with UVES at the VLT. The objects were selected from the full catalog to be accessible on the sky and to be bright enough to be observed in less than 3 hr, maximizing the number of observable objects. We thus sample the brighter two-thirds of the luminosity range covered by the clusters identified from the *HST* images. Whether this bias in absolute magnitude introduces others, toward either younger or more massive clusters, is at present unclear.

2.2. *Observations*

The VLT spectra were taken with UVES attached to Kueyen (UT2) during three nights of observation from 2001 December 9 to 11. All nights were clear with a seeing around 0.″8. UVES can work in parallel at blue and red wavelengths by using a dichroic beam splitter that divides the light from the object at the entrance of the instrument. Our main goal was to derive ages from the spectral region around the Balmer break and velocity dispersions from the calcium triplet. In order to also include the Hα line, we chose a nonstandard setting with the dichroic No. 2 and the cross-dispersers Nos. 2 and 4 centered on the wavelengths 4200 and 8000 Å. The resulting wavelength range is thus 3570–4830 Å in the blue arm; the red arm spectra are imaged on two CCDs, one covering 6120–7980 Å and the other one covering 8070–9920 Å. The length of the slit was 10″; the width was 1″. The slit was always oriented perpendicular to the horizon to minimize the effects of differential refraction. The spectral resolution is ≈35000 around the calcium triplet as measured from sky lines. This corresponds to a Gaussian dispersion of the instrumental line-spread function of 3.4 km s^{-1}. The pixel size in the reduced spectra is ∼0.07 Å.

Effective radii r_e for the clusters were derived from *HST* photometry in B04. They are smaller than 0.″2 for all observed clusters. Because the seeing disk is bigger than the effective radii, we essentially measure integrated properties. The observed NCs together with exposure times are listed in Table 1. For all objects in our sample, the *HST* images can be found in B02.

We also observed a number of template stars of known spectral types ranging from B to K and listed in Table 2. As explained in § 3.1, these are used to reliably measure the velocity dispersion of the NCs.

2.3. *Reduction*

The data were reduced with the UVES reduction pipeline, version 1.2.0, provided by ESO (see Ballester et al. 2001). For each observing night the following steps for preparing the calibration database were performed: first, using a physical model of UVES a first-guess wavelength solution was determined. Then, the order positions were identified from an order definition flat field. Next, the final wavelength calibration was done using a ThAr-lamp exposure. Finally, master bias and master flat fields were created from the median of five input frames each.

Cosmic-ray removal was done on the two-dimensional science frames by means of the MIDAS routine FILTER/COSMIC. The science frames were then bias-subtracted, and the inter-order background was subtracted by fitting a spline function to the grid of background positions. For each background position the median of pixels within a certain window was used

TABLE 2
STELLAR TEMPLATE WEIGHTS

Star (1)	Type (2)	m_V (3)	300 (4)	428 (5)	1042 (6)	1493 (7)	2139 (8)	3423 (9)	7418 (10)	7424 (11)	7793 (12)
HR 3611	B6 V	5.60	0.0	0.0	0.0	0.0	0.0	0.0	0.0	0.0	0.32
HR 3230	A1 V	6.52	0.26	0.31	0.63	0.75	0.76	0.36	0.79	0.73	0.19
HR 3473	A5 V	6.11	0.12	0.0	0.0	0.0	0.0	0.0	0.0	0.0	0.0
HR 3070	F1 V	5.78	0.0	0.0	0.0	0.0	0.0	0.0	0.0	0.0	0.0
HR 3378	G5 III	5.87	0.0	0.0	0.0	0.0	0.0	0.0	0.0	0.0	0.0
HR 1167	G8 III	6.49	0.0	0.59	0.25	0.18	0.22	0.50	0.8	0.23	0.48
HR 1216	K2 III	5.93	0.61	0.09	0.12	0.07	0.02	0.13	0.13	0.4	0.01

NOTE.—Cols. (4)–(12) are labeled by NGC number and contain the relative weights of the template stars that contribute to the velocity dispersion fit, as determined by the fitting code.

as the measurement at that point. The flat-fielding was not done on the two-dimensional raw frames, but after extraction for each order on the extracted one-dimensional spectrum. The extraction can be done using either an optimal extraction method or a simple average over a predefined slit. For our high signal-to-noise ratio (S/N) data, we found that the optimal extraction method shows quality problems appearing as sudden spikes and ripples, especially in the blue. We were able to recover almost the same S/N with the average method also for the lower S/N spectra by fine-tuning the extraction parameters (position and width of the extraction slit and position of the sky windows). For consistency we therefore decided to extract all spectra with the average method. S/N values around the calcium triplet are listed for all spectra in Table 1.

It is important to note that background light from the galaxy disk underlying the NC is subtracted together with the sky background during extraction, so that the contamination from noncluster light is reduced. However, not all the disk light is subtracted, because the disk brightness is not generally constant with radius. To quantify the fraction of cluster light in the final spectra, we simulate our UVES observations using the high spatial resolution *HST* data. The *I* band, at an effective wavelength of 8000 Å, will yield a correct fraction for the wavelength of the Ca triplet. We convolve the *HST* images with a Gaussian of 0.″8 seeing. From the known slit position we can derive the position of the spectroscopic object and sky windows on the *HST* image. The expected total flux in the reduced object spectrum $F_{\rm spec}$ is then computed by subtracting the flux in the sky windows from that in the object window. The total flux $F_{\rm cl}$ from the cluster alone is known from the magnitudes given in B02. The fraction f of the total cluster flux that falls within the spectroscopic object window is

$$f = \frac{1}{4}\left[\mathrm{erf}(x/\sqrt{2}\sigma) - \mathrm{erf}(-x/\sqrt{2}\sigma)\right] \times \left[\mathrm{erf}(y/\sqrt{2}\sigma) - \mathrm{erf}(-y/\sqrt{2}\sigma)\right], \quad (1)$$

where

$$\sigma = \sqrt{\sigma^2_{\rm PSF} + \sigma^2_{\rm cluster}}. \quad (2)$$

Here x is half the size of the spectroscopic object extraction window along the slit and y is half the slit width. In this equation it is assumed for simplicity that the point-spread function (PSF) and cluster are well approximated by Gaussians with the correct FWHM. Finally, the contamination from noncluster light (NCL) in the extracted spectra (as given in Table 1) is

$$\mathrm{NCL} = 1 - \frac{fF_{\rm cl}}{F_{\rm spec}}. \quad (3)$$

3. DATA ANALYSIS

3.1. *Measurement of the Velocity Dispersion*

Stellar kinematic analyses of unresolved populations assume that an observed galaxy spectrum can be represented by the convolution of one or several stellar templates with a certain broadening function, often approximated as a Gaussian. The line width in the template spectra represents both the intrinsic width of the stellar photospheric lines and the instrumental broadening. The galaxy spectra of unresolved populations are presumed to differ only by the additional Doppler broadening, reflecting the velocity dispersion of the stars. For massive galaxies this last broadening dominates the intrinsic line width by a wide margin, and the estimated velocity dispersion is nearly insensitive to the choice of templates. This is not the case, however, for the objects in our sample, as we show that their measured velocity dispersions range from only 13 to 34 km s^{-1}.

We use a code that matches simultaneously a linear combination of template stars and the width of a single Gaussian broadening function. No Fourier transform is involved, as the code works directly with the measured spectra (see Rix & White 1992). Each pixel in the spectrum is weighted with its specific error during the fitting process. It is particularly important to take templates observed with the same instrumental setup as the science targets to avoid systematic errors, i.e., resolution mismatch interpreted as velocity dispersion differences. We use the seven template stars ranging from type B to K listed in Table 2. An inherent strength of the code is the ability to determine an optimized template from the linear combination of the available template stars. It is thus possible to account to some extent for the influence of the generally young mean age of the clusters on the intrinsic width of the absorption lines. A further advantage of the direct fitting in pixel space is that masking spectral regions, which is essential to our analysis, is straightforward.

Velocity dispersions are measured from the spectral region around the calcium triplet. We choose the largest region that is relatively free of telluric absorption bands and emission lines (8400–8900 Å; see below). The calcium triplet region includes not only the very prominent Ca II lines but also several other metal lines, whose width can be measured at our S/N. Other regions of common use to measure velocity dispersions (e.g., the CO band head in the infrared, as in, e.g., Böker et al. 1999, or the

region around 5100–5500 Å, as in Maraston et al. 2004) are not covered by our data. However, we also investigated two other regions of the observed spectrum, namely 6385–6525 and 4380–4800 Å, which are also free of telluric lines and do have other metal lines. The measured velocity dispersions agree to within 15% for those clusters where the S/N of the metal lines is sufficient to measure σ reliably. These are most notably the old clusters NGC 300 and NGC 428 and the high-S/N spectrum of NGC 7793. The calcium triplet has been shown to give reliable results for old stellar populations, e.g., in elliptical galaxies, by a variety of authors (e.g., Dressler 1984; Barth et al. 2002). However, as the analysis of the blue parts of the UVES spectra shows (Walcher et al. 2003), some of our objects have ages between 10^7 and 10^8 yr. Unfortunately, kinematic measurements are more complicated in populations significantly younger than 1 Gyr. Although the intrinsic width of the Ca triplet changes only slightly from main-sequence K to late F stars, for earlier types rotation and temperature cause the intrinsic width to increase rapidly. Further, in supergiants the damping wings of the Voigt profile become increasingly important because of the depth of the lines. It is in this context very unfortunate that we do not have a supergiant in our stellar template set. A further complication comes from the presence of intrinsically broad absorption lines from the Paschen series. Especially the lines Pa 16, Pa 17, and Pa 13 (8504.8, 8547.7, and 8667.9 Å, respectively) overlap with the Ca triplet lines. All of these effects lead to an overestimation of the velocity dispersion, if only measured from main-sequence stars. We thus need to analyze carefully the composition of the stellar populations in consideration. On the other hand, the intervening Paschen absorption lines provide an additional diagnostic tool for the age of the population. With good S/N in the spectra this can be used to constrain the optimal stellar template mix for the velocity dispersion determination. For all spectra we also have age information from the blue parts of the spectrum. While we use this information for the assessment of age-related problems, a more detailed analysis of the age composition of the clusters will be published in a forthcoming paper (C. J. Walcher et al. 2005, in preparation).

To assess the influence of the calcium triplet problems we follow two different approaches concerning the wavelength coverage of the velocity dispersion fits. In what we call "case 1" we use almost the full wavelength range between 8400 and 8900 Å as the fitting region. Unfortunately, the Ca triplet line at 8498 Å falls onto a CCD defect in the interval from 8470–8510 Å, which we exclude from all fits. We thus cover the two Ca lines at 8542 and 8662 Å and further metal lines, mostly Fe I. For case 1, the χ^2 that measures the quality of the fit is dominated by the calcium triplet lines. In "case 2" we use only the weaker metal lines of Fe and Si in the region for the fit. These are not as deep as the Ca II lines and tend to disappear in earlier type stellar spectra, so that they are much less affected by the systematic problems with the Ca triplet mentioned above. Figure 1 illustrates the spectral region in use. Case 2 clearly is limited by S/N in the galaxy spectra and increases possible systematic uncertainties because of metallicity mismatches. So we divide our sample into two bins, the "old" ($\gtrsim$1 Gyr) and the "young" ($<$1 Gyr) bins. The three clusters NGC 300, NGC 428, and NGC 3423 are old, and we therefore use the case 1 value because of the larger fitting region and thus better constrained fit. In the other six clusters, the young clusters, we prefer the case 2 values because they avoid the systematic uncertainties related to the Ca triplet. For all cases the velocity dispersion for case 1 is higher than for case 2. However, the mean offset between case 1 and case 2 is 4.3 km s^{-1} in the old bin but 11.6 km s^{-1} in the young bin, demonstrating the influence of age on the velocity dispersion as measured from the Ca triplet. Table 2 quotes the weights that the fitting code attributes to every single template star in its best-fitting composite template. Note that the division in an old and a young bin is borne out by the lower contribution of A stars to the three NCs NGC 300, NGC 428, and NGC 3423. Table 3 contains only the finally adopted velocity dispersion. Formal random errors are available from χ^2 statistics. However, these do not include any systematic uncertainties and are therefore not particularly realistic. Useful error estimates are hard to obtain with all the complications from systematic effects just discussed. Typical systematic uncertainties from fitting different initial templates and different subsets of the available template set are of the order of 15%. These are the errors we quote in Table 3.

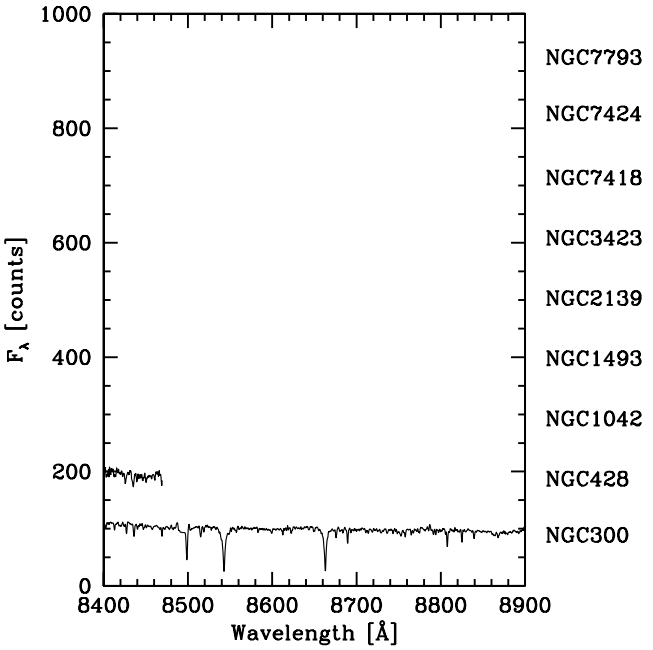

FIG. 1.—Region around the calcium triplet used for the velocity dispersion measurements. For better presentation, the spectra have been clipped to exclude residuals from sky lines and binned over 3 pixels. Fluxes have been arbitrarily adjusted to fit into the plot. Almost the full region was used for case 1 fitting, excluding only the region from 8470 to 8510 Å because of a CCD defect. The dotted lines show the six metal lines used for case 2 fitting.

The measured velocity dispersion is the luminosity-weighted mean of the two components (disk and NC) that contribute to the light inside the ground-based aperture. Section 3.3 details how we account for this in our dynamical modeling. Typical disk velocity dispersions are around 30 km s^{-1} for early-type spirals (Bottema 1993). The Sm galaxy UGC 4325 has a central disk velocity dispersion of 19 $\pm$ 2 km s^{-1} (Swaters 1999). Velocity dispersion of cluster and disk could therefore be of comparable magnitude.

3.2. *Surface Brightness Profiles*

For the purposes of dynamical modeling we need PSF deconvolved surface brightness profiles of the NCs and the surrounding galaxy disk. To this end we derive *I*-band surface brightness profiles from the *HST*/WFPC2 imaging data described in B02. Data reduction has been described there and will not be repeated here. While B02 inferred surface brightness profiles from their data, they did not perform PSF deconvolution. However, accurate effective radii for most NCs in the B02

TABLE 3
Dynamical Quantities

Galaxy (1)	σ (km s^{-1}) (2)	$\log(L_I)$ ($L_\odot$) (3)	$M/L_I^{\rm dyn}$ (4)	$\log(M)$ ($M_\odot$) (5)
NGC 300.....	13.3 ± 2.0	6.21 ± 0.20	0.65 ± 0.20	6.02 ± 0.24
NGC 428.....	24.4 ± 3.7	6.89 ± 0.04	0.42 ± 0.13	6.51 ± 0.14
NGC 1042.....	32.0 ± 4.8	6.81 ± 0.16	0.50 ± 0.15	6.51 ± 0.21
NGC 1493.....	25.0 ± 3.8	6.89 ± 0.05	0.31 ± 0.09	6.38 ± 0.14
NGC 2139.....	16.5 ± 2.5	6.69 ± 0.16	0.17 ± 0.05	5.92 ± 0.20
NGC 3423.....	30.4 ± 4.6	6.37 ± 0.06	1.46 ± 0.44	6.53 ± 0.14
NGC 7418.....	34.1 ± 5.1	8.13 ± 0.13	0.45 ± 0.14	7.78 ± 0.19
NGC 7424.....	15.6 ± 2.3	6.20 ± 0.06	0.78 ± 0.23	6.09 ± 0.14
NGC 7793.....	24.6 ± 3.7	7.08 ± 0.05	0.64 ± 0.19	6.89 ± 0.14

Notes.—Col. (1): Galaxy name. Col. (2): Measured velocity dispersion with systematic error. Col. (3): Logarithm of the *I*-band cluster luminosity (from B02). The errors we use here are somewhat larger than quoted in B02 because they include the uncertainty of 0.1 mag due to difficulties in determining the outer radius of the cluster. Cols. (4) and (5): M/L (in solar *I*-band units) and $\log(M) = \log[(M/L)L]$ of the cluster as derived from the dynamical modeling.

sample have been measured for most objects in our sample in B04. For their analysis, B04 used the software package ISHAPE (Larsen 1999) to fit PSF-convolved King or Moffat profiles with different concentration indices to the data. We here present a new analysis with the GALFIT routine (Peng et al. 2002). The reasons to repeat the exercise with a different software are twofold:

1. Three out of the nine clusters in our present sample are placed in galaxy centers with irregular morphologies. As the fits from ISHAPE were therefore deemed unsatisfactory in B04, they were rejected at the time. A careful reexamination with GALFIT, however, yielded useful results at least for the purposes of our dynamical modeling.
2. In B04 the main goal was to derive accurate effective radii for the clusters alone, implying the use of a single component for the cluster profile only. This one component then does not represent the light profile outside the cluster radius, called R_u in B04. However, we here need the full deconvolved surface brightness profile, including the background galaxy, for the dynamical modeling. GALFIT allows us to model the cluster and its surroundings with an unlimited number of different components, thereby optimizing the fit to the surface brightness profile at all radii.

In brief, GALFIT convolves a two-dimensional model that has a user-defined number of different analytic components (e.g., Sersic, Gaussian, exponential, and constant background) with a user-supplied PSF and finds the particular parameter set that best describes the observations. In most cases we use an exponential for the galaxy disk and a Sersic profile for the cluster. Very few complicated cases require more components. For example, the most complicated case is NGC 2139, which needs five components to be fitted well. That means a constant background, one exponential for the overall galaxy disk, one exponential component for the bar, one Sersic component for some extended emission around the cluster, and one Sersic component for the cluster itself. Only one galaxy (NGC 7418) shows evidence for large amounts of dust. For this galaxy only, we therefore created a dust mask that was used to cover the region to the west of the NC for the GALFIT fit. We use the same PSFs as in B04, constructed using the Tiny Tim software (Krist & Hook 2001). Our dynamical modeling, described in § 3.3, is based on the assumption of spherical symmetry. The calculations start from the projected surface brightness profile. For this purpose we use the best-fitting analytic GALFIT model for each galaxy to calculate the azimuthally averaged surface brightness profile. The averaging is done over circles that are centered on the component that we identify as the NC. Figure 2 shows the derived "deconvolved" surface brightness profiles in comparison to the nondeconvolved ones from B02. While the general shape agrees well, all deconvolved profiles are more concentrated, as expected. Note also that the size of a pixel on the PC chip is 0.″04555. The shape of the profile at smaller radii is therefore not well constrained.

Although the different components of the GALFIT fits were not chosen to have any physical meaning, it turns out that the least spatially extended component can be identified with the NC, except for one case (in NGC 7418 the cluster is represented by an addition of one Sersic and one Gaussian profile with very similar effective radii). When comparing effective radii derived for the NCs under this identification with those determined with ISHAPE, we find that they agree well to about 30%. However, strictly speaking the effective radii from ISHAPE are in general more reliable than the ones derived from the GALFIT models, because the extended wings of Sersic profiles may change the total luminosity content (and therefore the effective radius) of a model significantly with only small changes of the Sersic *n*-parameter. In contrast, King profiles do have a cutoff at large radius. B04 showed that the effective radius of the NCs is then well constrained, independent of uncertainties in their exact spatial profile.

3.3. *Dynamical Modeling*

The luminosity L, effective radius r_e, and line-of-sight velocity dispersion $\sigma_{\rm obs}$ are known for each of the clusters in our sample. It follows from simple dimensional arguments that the cluster mass-to-light ratio M/L is given by

$$M/L = \alpha \sigma_{\rm obs}^2 r_e / GL, \tag{4}$$

where G is the gravitational constant. The dimensionless constant α is determined by the density and velocity distribution of the cluster, and by the spatial area incorporated in $\sigma_{\rm obs}$. If $\sigma_{\rm obs}$ corresponds to the mass-weighted average dispersion of the entire cluster, then generally α is of order $\approx$10 by virtue of the virial theorem. For example, in this situation a spherical isotropic King (1962) model with concentration $c = 2$ has $\alpha = 9.77$. The value of α can be adjusted to account for the fact that not all of the cluster stars contributed to the observed spectrum because of the finite slit width, extraction aperture size, and PSF FWHM of the observations. However, we are dealing with clusters that reside in galaxy centers; therefore, application of equation (4) does not generally give accurate results. It ignores the fact that some of the light in the observed spectrum actually came from stars in the disk, rather than in the cluster (see the contamination fractions in Table 1). Most importantly, equation (4) ignores the gravitational potential of the disk. This is important, as is most easily seen for stars in the outskirts of the cluster. For a model of a cluster in isolation (such as a King model) these stars would have a dispersion profile that falls to zero at some finite radius. However, in reality these stars will behave as test particles in the gravitational potential of the disk. Their dispersion will therefore not fall to zero, but will instead converge to the same dispersion that the disk stars have. As a result

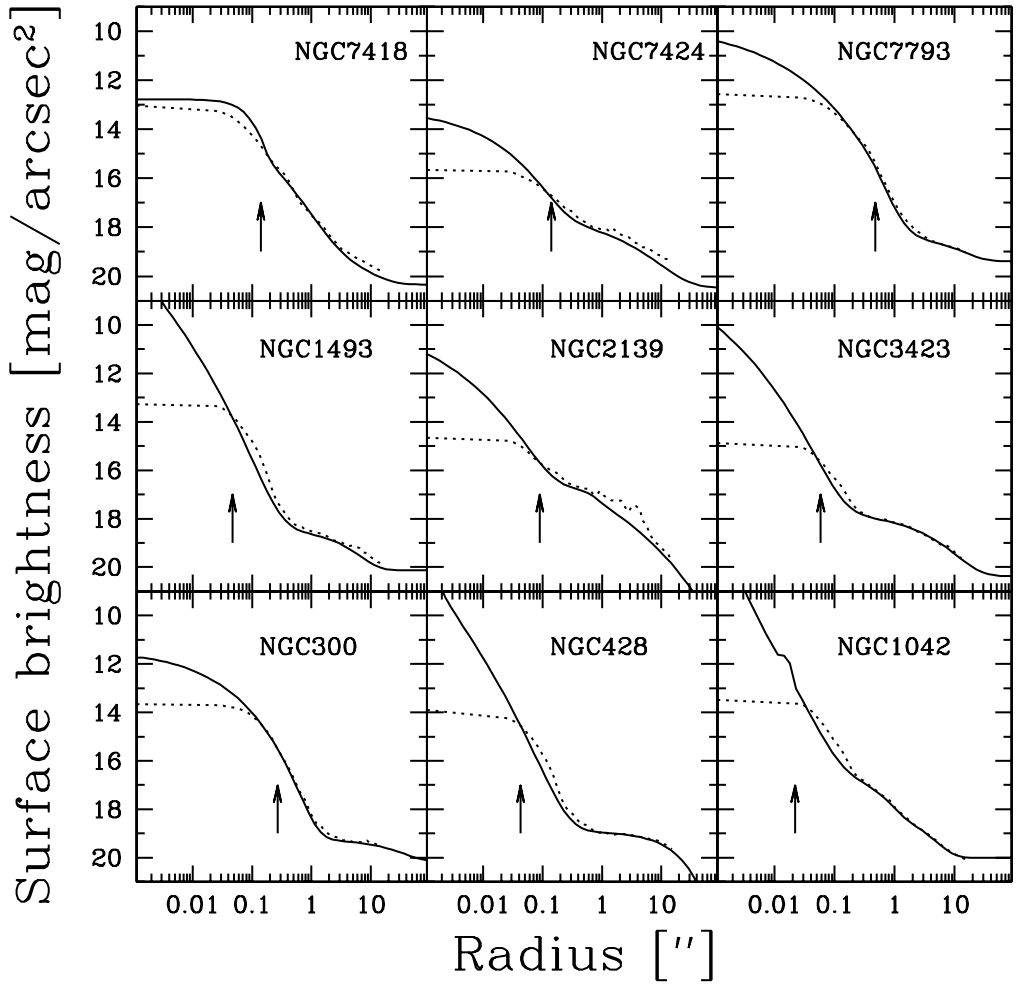

FIG. 2.—*I*-band surface brightness profiles (i.e., deconvolved from the PSF) obtained for the combined NCs and stellar disks in our present sample with GALFIT (*solid line*) compared with the nondeconvolved profiles obtained directly from the *HST* image (*dotted line*; from B02). The arrow corresponds to the effective radius of the star cluster. Note that the profile shapes agree reasonably well, but the deconvolved ones are always somewhat more concentrated toward the NC. Small differences between the profiles at large radii are due to differences in the methods used for model fitting and azimuthal averaging. These do not affect our dynamical modeling results.

of this effect, equation (4) tends to overestimate the cluster M/L. In practice, we found for our sample that the results from equation (4) are in error by factors of up to 5. For accurate results it is therefore important to model the galaxies in more detail.

We adopt an approach based on the Jeans equation for a spherical system. The details of this approach are described in van der Marel (1994). We start with the deconvolved galaxy surface brightness profile, obtained with the GALFIT software as described in § 3.2, to which we fit a smooth parameterized profile as in Geha et al. (2002). This profile is then deprojected using an Abel integral under the assumption of spherical symmetry. With an assumed constant $M/L = 1$ (in solar units) this yields a trial three-dimensional mass density $\rho(r)$. Solution of Poisson's equation yields the gravitational potential $\Phi(r)$, and the subsequent solution of the Jeans equation yields the three-dimensional velocity dispersion profile $\sigma(r)$. Luminosity-weighted projection along the line of sight gives the projected velocity dispersion profile $\sigma_p(R)$. Convolution with the observational PSF and integration over pixels along the slit yields the predicted velocity dispersion profile along the slit. On modeling the extraction apertures and background subtraction procedures that were used for the actual observations, this yields the predicted dispersion $\sigma_{\rm pred}$. The trial M/L ratio is then adjusted to $M/L = (\sigma_{\rm obs}/\sigma_{\rm pred})^2$ to bring the predictions into agreement with the observations. The fractional random error on the inferred M/L is twice the fractional random error on $\sigma_{\rm obs}$. The M/L values and their uncertainties thus obtained for all the sample NCs are listed in Table 3. The masses obtained by multiplication with the luminosities from B02 are also listed in the table. Errors on the masses include the errors on the luminosities as quoted in B02 and the error estimate on the velocity dispersion. In § 3.1 we found that use of the calcium triplet lines for young clusters yields velocity dispersion values that are $\approx$10 km s^{-1} higher than the ones we have adopted. As explained there, we believe that the calcium triplet lines give biased results for young stellar populations. Nonetheless, if one were to adopt those results anyway, then this would translate into a factor of 2 increase in mass for a cluster with a velocity dispersion of 20 km s^{-1}.

Although our results are significantly more accurate than those obtained with equation (4), it should be kept in mind that there are some remaining uncertainties. First of all, each system is assumed to be spherical. This is probably quite accurate for the cluster, but much less so for the disk. However, this is a reasonable lowest order approximation given that our only application is to an extraction aperture on the center. Here there is zero net rotation, and the disk is generally not the dominant

contributor to the observed light. Construction of fully axisymmetric models would be more accurate, but this is considerably more complicated and beyond the scope of the present paper. A second caveat on the adopted approach is that we assume that the cluster and the disk have the same M/L. If in reality the components have different M/L values, then one would expect

$$(M/L)_{\rm inferred} \approx (1-f)(M/L)_{\rm cluster} + f(M/L)_{\rm disk}, \qquad (5)$$

where f is the disk light contamination fraction listed in Table 1. We used the formalism described in Geha et al. (2002) to calculate several test models for one of the sample galaxies, in which we assumed different values for $(M/L)_{\rm cluster}$ and $(M/L)_{\rm disk}$. The results confirm equation (5). Thus our inferred M/L values are a weighted average of all the light in the extraction aperture. While for some galaxies this is almost exclusively light from the NC, this is not true for all galaxies.

4. DISCUSSION

The combination of spectroscopic and photometric data enables us to examine the structural properties of nuclear star clusters and their relation to other star clusters.

4.1. *Comparison to other Dynamically Hot Systems*

Dynamically hot stellar systems are defined by three observable quantities (neglecting the effects of nonhomology): velocity dispersion σ_e, effective radius r_e, and effective surface brightness I_e. The total luminosity and mass are related to these quantities according to $L = 2\pi r_e^2 I_e$ and equation (4). Dynamically hot systems satisfy a variety of correlations between their fundamental quantities, generally known under the keyword "fundamental plane." Any derived quantities will therefore also correlate. A popular way to view these relationships is κ-space (Bender et al. 1992). The κ-parameters are defined in terms of the fundamental observables so that κ_1 is related to mass, κ_3 is related to M/L, and κ_2 is related to the product of M/L and the third power of the effective surface brightness. Elliptical galaxies fall on a fundamental plane that is seen edge-on when viewed as κ_1 versus κ_3 and is seen face-on when viewed as κ_1 versus κ_2. Intrinsic age spreads, however, complicate the interpretation in κ-space, because κ-parameters are defined using luminosity surface density. Here we have done detailed modeling that provides mass and M/L directly of our sample NCs. We therefore choose to work with the more fundamental properties, rather than resort to κ-space.

In Figure 3 we plot effective projected mass density [$\Sigma_e \equiv (M/L)I_e$] versus mass. This is similar, but not identical, to a plot of κ_1 versus κ_2 (discussions of the latter that are of relevance to the present topic can be found in Geha et al. 2002 and Martini & Ho 2004). We plot a wide variety of different dynamical systems. Galaxy-sized systems fill the bottom right corner of the plot. Here small skeletal triangles show galaxy-type systems from the compilation in Burstein et al. (1997). The dwarf spheroidal (dSph) galaxies have been specially marked with additional open triangles. M32, the nearest compact elliptical galaxy, is marked with an open pentagon filled with a star. The nucleated dE galaxies of the Virgo Cluster from Geha et al. (2002) are represented by open squares filled with a cross. Stellar clusters, on the other hand, fall on a well-defined band in the left of the plot. Here NCs are represented by filled squares. The nuclei of dEs in Geha et al. (2002) are shown as open squares. Small stars show the locus of Milky Way GCs. Structural parameters (r_e and total V luminosities) of 108 Galactic GCs are

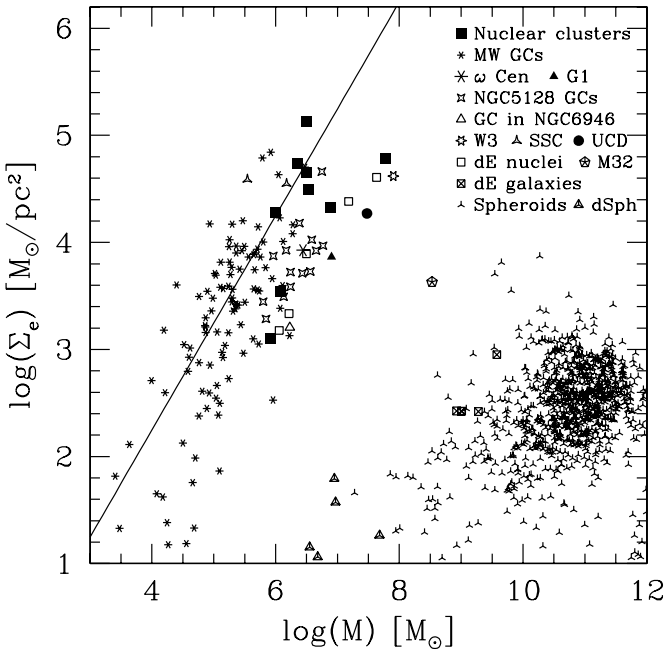

FIG. 3.—Mean projected mass density inside the effective radius against the total mass. This is similar to face-on view of the fundamental plane. Symbols represent different types of dynamically hot stellar systems. NCs occupy a region together with different types of massive stellar clusters and are well separated from any bulge. The solid line represents the locus of clusters with constant radius, α pc.

derived from the online catalog of King model parameters maintained by W. E. Harris (Harris 1996). Total cluster masses and related derived quantities then follow from applying V-band mass-to-light ratios computed by D. McLaughlin & R. P. van der Marel (2005, in preparation) using the population synthesis code of Bruzual & Charlot (2003). These population synthesis M/L values generally compare quite well with the dynamical M/L_V derived by McLaughlin (2000) for a subsample of 40 globular clusters with measured velocity dispersions; see D. McLaughlin & R. P. van der Marel (2005, in preparation) for more details. The most massive GC of the Milky Way, ω Cen (NGC 5139), is specially marked as a big star. G1, the most massive GC of M31 (Meylan et al. 2001; Baumgardt et al. 2003), is also pointed out as a filled triangle. The most massive GCs of Cen A (NGC 5128; Harris et al. 2002; Martini & Ho 2004) are represented as starred crosses. Two SSCs in M81 with dynamical mass estimates from McCrady et al. (2003) are shown as starred triangles. These were selected to be particularly bright and hence are not representative for the total SSC population. The young, peculiar GC in NGC 6946 described in Larsen et al. (2001) is denoted by an open triangle. It resides in an Sc galaxy in the disk at 5 kpc from the center and is surrounded by an extended star-forming region. The cluster is extremely luminous ($M_V = -13.2$) and relatively massive ($1.7 \times 10^6\ M_\odot$). Also shown is the most massive cluster known, W3, in the merger remnant galaxy NGC 7252 (Maraston et al. 2004). We additionally plot the approximate locus of the ultracompact dwarf galaxies from Drinkwater et al. (2003) as a filled circle. As these authors do not give numbers for each one of their objects, we plot only a mean of the range of values given in that paper. The solid line running through the cluster sequence represents a line of constant $r_e = 3$ pc, which is appropriate for Milky Way GCs.

Concentrating on the mass scale only, Figure 3 shows that NCs are more massive than the typical Milky Way GC by more

than 1 order of magnitude. While Milky Way GCs range from 10^4 to $10^6\,M_\odot$, NCs fall in the range 10^6–$10^7\,M_\odot$. Several extragalactic star clusters are, however, also found in this range. First, the GC system of Cen A extends the mass range of GCs by 1 order of magnitude. Then, several clusters that have been speculated to be the remaining nuclei of accreted satellite galaxies are also found in this mass range (e.g., ω Cen or G1). Further, the least massive galaxies, i.e., the dSph galaxies, are as massive as the most massive stellar clusters, showing that the stellar mass ranges of galaxies and star clusters overlap.

A clear distinction between clusters and galaxies, however, remains; dSph galaxies are less dense by 4 orders of magnitude than the most massive clusters. It is indeed striking that all massive clusters prolong the well-known GC sequence toward higher masses *and* higher densities. Nuclear star clusters fall well onto this sequence, while there is a wide gap in properties to the location of compact elliptical or bulge galaxies. Indeed, the later Hubble type a galaxy has, the more its bulge will become exponential and blend with the underlying disk (cf. MacArthur et al. 2003; Böker et al. 2003 and references therein), instead of remaining a small but distinct entity. Compact small bulges do not exist, or at least have not been observed so far. While at first sight a tempting hypothesis, because of their location at the centers of their host galaxies, a smooth evolutionary transition from NCs to bulges therefore seems highly unlikely, as there are no transition objects to fill the gap in Figure 3.

The well-defined cluster sequence also means that, independent of their different environment, nuclear star clusters follow scaling relations between mass and radius similar to all other types of star clusters. From their location in Figure 3 the ultracompact dwarf galaxies of the Fornax Cluster (Drinkwater et al. 2003) may well have to be treated as huge star clusters. There is only a hint of a possible discontinuity in properties. While Milky Way GCs are consistent with a constant radius line, the cluster sequence may bend over at a characteristic scale of $\approx 10^6\,M_\odot$, in the sense that more massive clusters have larger effective radii. This is analogous to the so-called zone of avoidance in the κ-space cosmic metaplane, as discussed, e.g., in Burstein et al. (1997). Those authors infer an upper limit to the three-dimensional luminosity density that scales roughly as $\sim M^{-4/3}$. In our plot of two-dimensional mass density, the empty top right region of Figure 3 suggests $\Sigma_{\max} \sim M^{-1/2}$.

4.2. *Are the Centers of Bulgeless Galaxies Particularly Conducive to Massive Cluster Formation?*

Many authors have shown that the most massive GCs can be the remaining stripped nuclei of accreted satellite galaxies. In this scenario a nucleated galaxy is stripped of all of its stellar envelope through tidal forces during a minor merger with a bigger galaxy, as, e.g., our Milky Way. The nucleus, however, is compact enough to survive and remains in the halo of the bigger galaxy as a massive GC. This scenario has been proposed for ω Cen (see, e.g., Bekki & Freeman 2003 and references therein), G1 orbiting M31 (e.g., Meylan et al. 2001), the ultracompact dwarf galaxies in the Fornax Cluster (Drinkwater et al. 2003), and others. In Figure 3, the average properties of NCs are similar to those of the Fornax UCDs and the nuclei of dE galaxies. Further individual GCs, such as ω Cen and G1, have similar properties as well. The average properties of the Milky Way and NGC 5128 GC sample, however, are different. One might therefore speculate that NCs, the nuclei of dEs, and UCDs are basically the same thing, albeit in different evolutionary stages of their host galaxy. Remember, however, that all of the involved samples are biased. The Milky Way GC sample is probably not representative of all GC systems, in that it lacks the most massive ones, as shown by the measurements of the most luminous GCs of NGC 5128. Our own NC sample only covers the brighter two-thirds of the luminosity function of NCs and might therefore be biased to higher masses. In the case of UCDs, more compact and less luminous specimens might exist without being detected.

Taking Figure 3 at face value, however, and accepting the merger hypothesis for the most massive clusters, it seems as though star clusters formed in the nuclei of galaxies are, as a class, more massive and more dense than the GC class. It would then be natural to attribute these special properties to their location in the center of their host galaxy at formation time. Indeed, to reach the very high space densities that are found in these clusters in one star formation event, an extremely high efficiency of star formation is necessary, implying high gas pressure from the surroundings of the forming cluster. Otherwise the gas blown out by feedback will invariably puff up the cluster to a much bigger size (e.g., Geyer & Burkert 2001). High space densities in a quiescent environment, as is the case in the centers of late-type spirals, can be reached more naturally by invoking repeated bursts of star formation from the repeated infall of fresh gas. Each infalling cloud will turn some percentage of its mass into stars inside the boundaries of the cluster—thus increasing the space density—before blowing out the remainder through feedback. Rather than one single event, star formation in a nuclear star cluster is therefore likely to be a repetitive process.

That sufficient gas can be transported to the center of the spiral disk has been demonstrated by Milosavljevic (2004) under the assumption of a divergent dark matter density profile. For very late type galaxies, however, this scenario does not work well. Matthews & Gallagher (2002) find that the rotation curves of very late type spirals are nearly linear, implying a constant surface mass density and a harmonic potential, where the gravitational vector vanishes at the center. It therefore remains unclear why the centers of bulgeless galaxies would be special places, conducive to the formation of stellar systems with extreme physical properties.

4.3. *Phase-Space Densities*

Figure 4 shows f_h, the characteristic phase-space density inside the half-mass radius, against mass for the same types of stellar systems as used in Figure 3. We define f_h using the half-mass radius r_h, total mass M, and measured velocity dispersion σ according to

$$f_h = \frac{\rho_h}{\sigma^3} = \frac{M}{2}\frac{1}{(4/3\pi) r_h^3 \sigma^3} \propto r_h^{-2}\sigma^{-1}. \tag{6}$$

This quantity can be calculated for various dynamically hot systems using the literature mentioned in § 4.1. The projected effective radii r_e have been converted to three-dimensional half-mass radii r_h by the approximate relation $r_e = 0.75 r_h$ (see Spitzer 1987, p. 12). No correction was applied to the velocity dispersions.

In addition, the lines in Figure 4 show fits to two different subsets of the systems. The dotted line is a fit to Milky Way GCs only, where $\log(f_h) = 2.57 - [0.5 \log(M)]$. The virial theorem dictates that $M \propto r_h \sigma^2$. The fit is therefore a line of constant r_h, where $r_h \approx 8$ pc. The solid line is a fit to the galaxy-type systems, where $\log(f_h) = 3.44 - [1.1 \log(M)]$ (excluding the Virgo dE,N

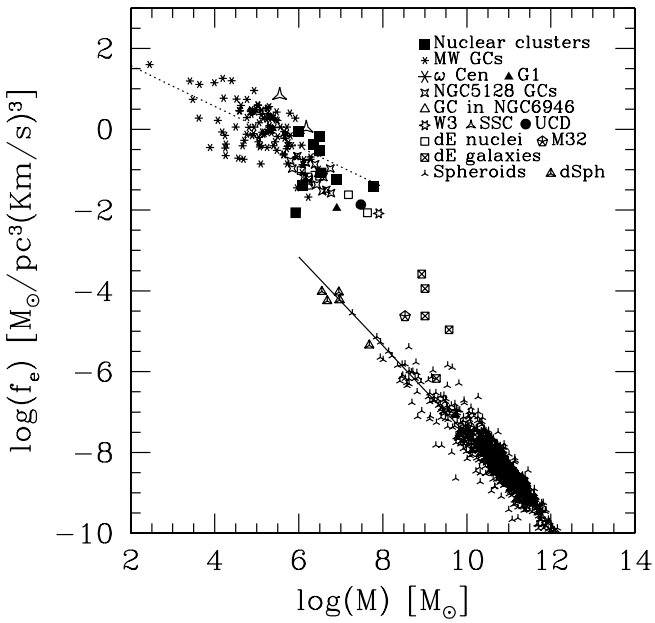

FIG. 4.—Characteristic phase-space density f_h, i.e., the mean phase-space density inside the half-mass radius r_h for the same dynamically hot systems as in Fig. 3. The dotted line represents the locus of systems that obey the virial theorem and have constant radius r_h. The solid line represents a locus of systems that obey the virial theorem as well as a Faber-Jackson (1976) type relationship of the form $M \propto \sigma^{3.33}$.

from Geha et al. 2002). This fit implies that $M \propto \sigma^{3.3}$, which is a Faber-Jackson (1976) type relationship.

Again, as in § 4.1, NCs fall on the locus of typical massive star clusters. There is a clear discontinuity to galaxies, but more importantly a change of slope, thereby reinforcing the statement that nuclear star clusters are typical massive star clusters (and not progenitors of bulges).

On the other hand, the phase-space densities may be directly linked to star formation processes. Dynamical evolution is potentially not responsible for the slope observed in the cluster sequence, as there is no obvious trend with age, even though the ages of the involved clusters range from around 10^7 yr (SSCs; young massive cluster in NGC 6946) over 10^8 yr (some of the NCs; W3) to very old objects, such as the Milky Way GCs. A more detailed interpretation of this result clearly requires simulations of the formation of massive star clusters and NCs in particular.

4.4. *Formation of Intermediate-Mass Black Holes*

Because of their very high mass densities, NCs might be considered to be ideal candidates for fast core collapse and subsequent runaway merging of young massive stars, thus forming an intermediate-mass black hole. Comparison with relevant current models (Portegies-Zwart et al. 2004; M. Freitag 2004, private communication), however, shows that NCs do not fall into the appropriate region of parameter space. When inserting the typical values of NCs into equation (1) of Portegies-Zwart et al. (2004), we obtain a dynamical friction timescale of the order of 24 Myr for a 100 $M_\odot$ star, which is much longer than its lifetime. These stars will therefore explode as supernovae before reaching the center of the cluster and will not experience runaway merging. Less massive stars undergo weaker dynamical friction and are thus even less likely to reach the cluster center in an appropriate timescale for the formation of a black hole.

5. SUMMARY AND CONCLUSIONS

Most bulgeless, very late type galaxies have been shown to have photometrically distinct, compact nuclear star clusters (several parsecs in size) at their photometric centers, a stark contrast to the diffuse stellar disk around them. We determine the stellar velocity dispersion for nine such nuclear star clusters, derived from high-resolution spectra taken with UVES at the VLT. For observational reasons we sample the brighter two-thirds of the luminosity range covered by the clusters. In conjunction with light profiles from the WFPC2 camera on board *HST*, we also determine their masses. We find them to range from 8×10^5 to 6×10^7 $M_\odot$. The nine objects analyzed provide an order-of-magnitude increase in the number of available determinations, as the only mass known so far had been determined in IC 342 to be 6×10^6 $M_\odot$ (Böker et al. 1999).

The mass estimates show that as a class, these NCs in late-type galaxies have structural properties similar to the most massive known stellar clusters.

1. At around 5×10^6 $M_\odot$ their characteristic masses are much larger than those of Milky Way GCs, except ω Cen. They however fall into the same range as some of the most extreme stellar clusters observed so far, such as G1 in M31 or the most massive GCs of NGC 5128.

2. The properties of the NCs show that they are widely distinct from all bulges with measured structural parameters, by orders of magnitude in mass and radius.

3. Combining the mass estimates with their effective radii, we find NCs to be among the clearly distinct stellar systems with the highest mean mass density within their effective radius. Remarkably, although they lie in hugely different environments and thus presumably form in different ways, different sorts of star clusters follow the same mass-to-density and mass–to–phase-space density relations.

The combination of a galaxy center and a dynamically quiescent environment appears to be conducive to the creation of dense stellar systems with extreme physical properties. These results thus confirm that even in these very late type galaxies, of overall low stellar surface mass density, the center of the galaxy is "special." This leaves open the question of why some late-type galaxies seem not to have any such clusters. From their position in their host galaxies, the closest relatives of NCs appear to be the nuclei of dEs, which could be older and somewhat more diffuse analogs. However, assuming that massive GCs and the Fornax ultracompact dwarf galaxies are the remainders of accreted nucleated dwarf galaxies, all massive clusters with very high effective mass densities could have a common origin in the centers of galaxies.

In a companion paper (C. J. Walcher et al. 2005, in preparation) we will present further results from the blue parts of our UVES spectra yielding ages and star formation rates in our sample of nine NCs. We already remark here that the *I*-band mass-to-light ratios we find for NCs are smaller than the typical value of 1.2 (McLaughlin 2000) found for Galactic GCs and thus point to significantly younger objects.

C. J. W. would like to acknowledge intensive discussions with Marla Geha and the help of Dan Choon with literature research. C. J. W. also thanks STScI for hosting a long-term visit under a director's discretionary research fund grant. This research has made use of the SIMBAD astronomical database, created and maintained by the CDS, Strasbourg, as well as NASA's

Astrophysics Data System and the NASA/IPAC Extragalactic Database (NED), which is operated by the Jet Propulsion Laboratory, California Institute of Technology, under contract with the National Aeronautics and Space Administration. This research is based on observations collected at the European Southern Observatory, Chile [ESO Programme 68.B-0076(A)].

REFERENCES

Ballester, P., et al. 2001, UVES Pipeline and Quality Control User's Manual (Garching: ESO), http://www.eso.org/instruments/uves
Barth, A. J., Ho, L. C., & Sargent, W. L. W. 2002, AJ, 124, 2607
Baumgardt, H., Makino, J., Hut, P., McMillan, S., & Portegies Zwart, S. 2003, ApJ, 589, L25
Bekki, K., & Freeman, K. C. 2003, MNRAS, 346, L11
Bender, R., Burstein, D., & Faber, S. M. 1992, ApJ, 399, 462
Böker, T., Laine, S., van der Marel, R. P., Sarzi, M., Rix, H.-W., Ho, L. C., & Shields, J. C. 2002, AJ, 123, 1389 (B02)
Böker, T., Sarzi, M., McLaughlin, D. E., van der Marel, R. P., Rix, H.-W., Ho, L. C., & Shields, J. C. 2004, AJ, 127, 105 (B04)
Böker, T., Stanek, R., & van der Marel, R. P. 2003, AJ, 125, 1073
Böker, T., van der Marel, R. P., Mazzuca, L., Rix, H.-W., Rudnick, G., Ho, L. C., & Shields, J. C. 2001, AJ, 121, 1473
Böker, T., van der Marel, R. P., & Vacca, W. D. 1999, AJ, 118, 831
Bottema, R. 1993, A&A, 275, 16
Bruzual, G., & Charlot, S. 2003, MNRAS, 344, 1000
Burstein, D., Bender, R., Faber, S., & Nolthenius, R. 1997, AJ, 114, 1365
Carollo, M., Stiavelli, M., de Zeeuw, P. T., & Mack, J. 1997, AJ, 114, 2366
Carollo, M., Stiavelli, M., & Mack, J. 1998, AJ, 116, 68
Davidge, T. J. 2000, AJ, 119, 748
Dressler, A. 1984, ApJ, 286, 97
Drinkwater, M. J., Gregg, M. D., Hilker, M., Bekki, K., Couch, W. J., Ferguson, H. C., Jones, J. B., & Phillipps, S. 2003, Nature, 423, 519
Faber, S. M., & Jackson, R. E. 1976, ApJ, 204, 668
Geha, M., Guhathakurta, P., & van der Marel, R. P. 2002, AJ, 124, 3073
Gelatt, A. E., Hunter, D. A., & Gallagher, J. S. 2001, PASP, 113, 142
Geyer, M. P., & Burkert, A. 2001, MNRAS, 323, 988
Gordon, K. D., Hanson, M. M., Clayton, G. C., Rieke, G. H., & Misselt, K. A. 1999, ApJ, 519, 165
Harris, W. E. 1996, AJ, 112, 1487
Harris, W. E., Harris, G. L. H., Holland, S. T., & McLaughlin, D. E. 2002, AJ, 124, 1435
King, I. 1962, AJ, 67, 471
Kormendy, J., & McClure, R. D. 1993, AJ, 105, 1793
Krist, J., & Hook, R. 2001, The Tiny Tim User's Guide, Version 6.0 (Baltimore: STScI), http://www.stsci.edu/software/tinytim
Larsen, S. S. 1999, A&AS, 139, 393
Larsen, S. S., Brodie, J. P., Elmegreen, B. G., Efremov, Y. N., Hodge, P. W., & Richtler, T. 2001, ApJ, 556, 801
Long, K. S., Charles, P. A., & Dubus, G. 2002, ApJ, 569, 204
MacArthur, L. A., Courteau, S., & Holtzman, J. A. 2003, ApJ, 582, 689
Maraston, C., Bastian, N., Saglia, R. P., Kissler-Patig, M., Schweizer, F., & Goudfrooij, P. 2004, A&A, 416, 467
Martini, P., & Ho, L. 2004, ApJ, in press
Matthews, L. D., & Gallagher, J. S. 1997, AJ, 114, 1899
———. 2002, ApJS, 141, 429
McCrady, N., Gilbert, A. M., & Graham, J. R. 2003, ApJ, 596, 240
McLaughlin, D. E. 2000, ApJ, 539, 618
Meylan, G., Sarajedini, A., Jablonka, P., Djorgovski, S. G., Bridges, T., & Rich, R. M. 2001, AJ, 122, 830
Milosavljevic, M. 2004, ApJ, 605, L13
Peng, C. Y., Ho, L. C., Impey, C. D., & Rix, H.-W. 2002, AJ, 124, 266
Phillips, A. C., Illingworth, G. D., MacKenty, J. W., & Franx, M. 1996, AJ, 111, 1566
Portegies-Zwart, S. F., Baumgardt, H., Hut, P., Makino, J., & McMillan, S. L. W. 2004, Nature, 428, 724
Rix, H.-W., & White, S. D. M. 1992, MNRAS, 254, 389
Spitzer, L. 1987, Dynamical Evolution of Globular Clusters (Princeton: Princeton Univ. Press)
Stephens, A. W., & Frogel, J. A. 2002, AJ, 124, 2023
Swaters, R. A. 1999, Ph.D. thesis, Rijksuniv. Groningen
van der Marel, R. P. 1994, MNRAS, 270, 271
Walcher, C. J., Häring, N., Böker, T., Rix, H.-W., van der Marel, R., Gerssen, J., Ho, L. C., & Shields, J. C. 2003, in Coevolution of Black Holes and Galaxies, ed. L. C. Ho (Carnegie Obs. Astrophys. Ser.; Pasadena: Carnegie Obs.), http://www.ociw.edu/ociw/symposia/series/symposium1/proceedings.html)